Weakly Coordinating Organic Cations are Intrinsically Capable of Supporting CO_2 Reduction Catalysis

Sophia Weng, Wei Lun Toh, Yogesh Surendranath*

Department of Chemistry, Massachusetts Institute of Technology, Cambridge, Massachusetts 02139, United States

ABSTRACT: The rates and selectivity of electrochemical CO_2 reduction are known to be strongly influenced by the identity of alkali cations in the medium. However, experimentally, it remains unclear whether cation effects arise predominantly from coordinative stabilization of surface intermediates or from changes in the mean-field electrostatic environment at the interface. Herein, we show that Au- and Ag-catalyzed CO_2 reduction can occur in the presence of weakly coordinating (poly)tetraalkylammonium cations. Through competition experiments in which the catalytic activity of Au was monitored as a function of the ratio of the organic to metal cation, we identify regimes in which the organic cation exclusively controls CO_2 reduction selectivity and activity. We observe substantial CO production in this regime, suggesting that CO_2 reduction catalysis can occur in the absence of Lewis acidic cations and thus, coordinative interactions between the electrolyte cations and surface-bound intermediates are *not* required for CO_2 activation. For both Au and Ag, we find that tetraalkylammonium cations support catalytic activity for CO_2 reduction on par with alkali metal cations, but with distinct cation activity trends between Au and Ag. These findings support a revision in electrolyte design rules to include water-soluble organic cation salts as potential supporting electrolytes for CO_2 electrolysis.

INTRODUCTION

Electrochemical CO_2 reduction presents an attractive route for leveraging renewable electricity to drive the production of valuable fuels and commodity chemicals.[1] The local electrolyte and pH environment has been found to play a critical role in dictating the rate of the CO_2 reduction reaction (CO2RR) and in suppressing the parasitic hydrogen evolution reaction (HER).[2,3] Prior work has established that aqueous CO2RR rates and selectivity are strongly influenced by the identity of the supporting electrolyte cation, with catalytic activity increasing along the following trend: $Li^+ < Na^+ < K^+ < Cs^+$.[4–7] Indeed, for CO2RR studies on many different catalyst materials including Au, Ag, and Cu, it has been observed that the identity of the supporting electrolyte cation—a nominal spectator in the overall CO2RR—can have significant effects on CO2RR activity, with the rates varying by three-fold or greater across the series.[8,9]

Despite the widespread observation of cation effects on the CO2RR, the mechanistic basis for these trends remains the subject of intense debate.[8–20] Leading explanations put forward bifurcate into two broad categories: (a) cations induce changes to the mean-field electrostatic potential profile at the interface;[15–18] and (b) cations are involved in coordinative chemical interactions with adsorbed reaction intermediates.[11,12,19,21] The former electrostatic model postulates a sharper electrostatic potential drop in the presence of weakly hydrated cations such as Cs^+ relative to strongly hydrated ions such as Li^+.[15] The sharper potential drop is thought to preferentially stabilize polar adsorbed CO_2^* relative to non-polar adsorbed H* (**Figure 1a**, top).[16] In

contrast, the coordination model invokes that electrolyte cations act as Lewis acids that bind to the oxygen atoms of adsorbed CO_2^*, thereby promoting CO_2 activation (**Figure 1a**, bottom).[19,21] Since this coordination mode requires partial de-solvation of the ion, weakly hydrated cations such as Cs^+ are thought to interact more strongly with CO_2^*, resulting in a larger stabilizing effect. Critically, since all alkali metal cations can, in principle, participate in both electrostatic and coordinative modes of promotion (**Figure 1a**), trends across them are unable to distinguish the relative influence of each. Because each mode of promotion would motivate distinct approaches to electrolyte design, addressing this knowledge gap is critical for systematic improvements to CO2RR efficiency and selectivity.

Experimentally, CO_2 reduction has been extensively investigated in the presence of organic cations of various types, including surfactants[22,23], ionomer films[24–30], and cationic conjugate bases of superacids[31]. However, in all these studies, the organic cation is present as a minority constituent of the medium alongside either a super-stoichiometric excess of alkali metal cations for studies in neutral pH electrolytes (**Figure 1b**, top) or in the presence of super-stoichiometric excess of hydronium ions for studies in bulk acidic electrolyte[32]. Because these additives are only a minority constituent in the overall electrolyte, even if they are concentrated at the surface, it is challenging to definitively attribute CO_2 activation to these organic species versus alkali metal cations in the medium that may also be present at the surface (**Figure 1b**, bottom). Indeed, these systems often still display a strong sensitivity to the identity of the bulk alkali

metal cation[24], suggesting that alkali metal cations are still significantly influencing catalysis, despite the presence of the organic additive. Further complications are introduced when bulk acidic electrolyte is used, as the interface is invariably subject to a large pH gradient during catalysis,[33] obscuring the intrinsic mechanistic role of the organic cation in CO_2RR selectivity and/or efficiency. Consequently, these studies do not directly address whether organic cations on their own can foster CO_2 reduction catalysis. In principle, the foregoing modes of promotion can be better parsed by comparing CO_2RR efficiency and selectivity between alkali metal cations and far more weakly-coordinating[34] organic (e.g., tetraalkylammonium) cations. If weakly-coordinating cations can foster CO_2 reduction in an environment where the influence of alkali metal cations is excluded, this observation would lend credence to the electrostatic promotion mechanism over the coordination mechanism.
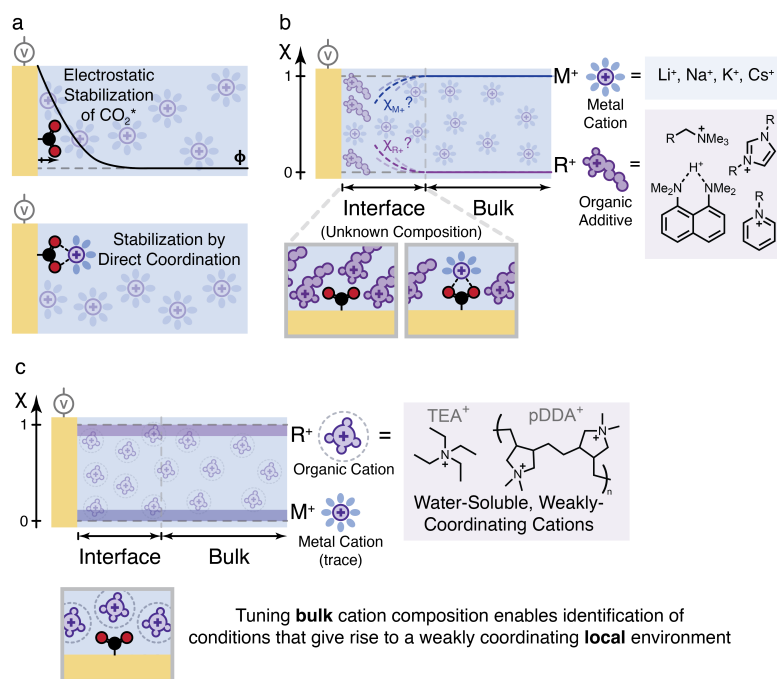
Figure 1. a, Depiction of the two modes of CO_2 activation by electrolyte cations proposed in the literature: electrostatic field-dipole stabilization of CO_2^* (top) and direct coordination of CO_2^* (bottom). **b**, Representation of the distribution of cations in an electrolyte containing majority alkali metal cations and minority organic additives. The concentration profile is depicted as a plot of cation mole fraction (χ) as a function of distance from the electrode surface (top). Molecular structures of some previously investigated organic additives are shown on the right.[22,24,26,31] In such systems, the interfacial composition may differ from the bulk and is largely unknown (bottom). **c**, Organic cations are employed herein in vast excess relative to trace alkali metal cations (top). Tuning the bulk cation composition enables us to identify conditions that give rise to a weakly coordinating local environment in which Lewis acid-base interactions between CO_2^* and electrolyte cations are inhibited (bottom). Molecular structures of the organic cations used in this study are shown on the right.

Herein, we examine CO_2 reduction catalysis in the limit of excess water-soluble weakly-coordinating tetraalkylammonium cations relative to trace alkali metal ions (**Figure 1c**). Activity trends for Au-catalyzed CO_2 reduction as a function of the ratio of the organic to metal cation reveal that the cation ratio at the interface can differ substantially from that of the bulk. These competition experiments expose regimes in which the catalytic activity arises predominantly from the organic cation. Within these regimes, we find that Au and Ag are both still competent catalysts for CO_2 reduction to CO with catalytic activity on par with that of alkali metal cations (Li^+, Na^+, K^+, and Cs^+). Our findings suggest that coordinative interactions between the electrolyte cations and surface-bound intermediates are not required for CO_2 reduction to CO, expanding the scope of viable electrolytes for fuel synthesis.

RESULTS AND DISCUSSION

### Methodology for minimizing adventitious alkali metal accumulation.

Trace alkali metal cations are common in electrochemical cells and can originate from a variety of sources. To minimize the possibility of adventitious accumulation of alkali metal cations at the working electrode interface over the course of an electrolysis experiment, we took several precautions. First, as metal-on-carbon catalysts often contain cation-exchange ionomer binders that can carry trace alkali ions as counter charges for their ionomer head groups, we opted to use gas diffusion electrodes prepared by the sputter deposition of Au and Ag on porous PTFE as our working electrodes (see **SI Methods** for details of electrode preparation and **Figures S2-S8** for characterization). This procedure generates metal-decorated gas diffusion electrodes free from ionomer binders and corresponding adventitious alkali ions. Second, to minimize adventitious ion

contamination from the counter electrode reaction, we employed a gold mesh or glassy carbon plate counter electrode separated from the working chamber by an anion-exchange membrane. Third, we employed a platinum-based reversible hydrogen electrode (RHE) in a separated compartment saturated with H_2 as the reference electrode (see **SI Methods** for details). The H_2/H^+ equilibrium on this electrode provides a stable reference potential on the time scale of the experimental measurements without introducing alkali metal cations present in common reference electrodes such as Ag/AgCl and Hg/HgSO4. As a result of these precautions, we found that alkali metal cations were only introduced from the electrolyte itself. Inductively coupled plasma mass spectrometry (ICP-MS) analysis confirms that cation populations were unchanged, within error, prior to and following electrolysis experiments for any given electrolyte (see **SI Methods** and **Table S4** for full details). With this carefully designed system in hand, we set out to measure the rate and selectivity of CO_2RR in aqueous media containing predominantly tetraalkylammonium cations to see if these weakly coordinating cations could foster CO_2 reduction catalysis.

CO_2 reduction is observed even when organic cations are in vast excess of alkali metal cations.

We began our investigations by establishing a baseline for CO_2RR catalytic activity with alkali metal cations in our custom electrochemical cell. To this end, we compared the product selectivity of Au- and Ag-catalyzed CO_2 reduction in bulk CO_2-saturated, 0.1 M $NaHCO_3$ electrolyte (pH 6.8). Gold and silver were specifically chosen because they both display cation-dependent CO_2 to CO reduction activity and generate a simple product distribution consisting predominantly of CO and H_2.[35,36] We studied the catalytic activity of both materials by coupling steady state chronoamperometry with an in-line gas chromatograph (GC) to quantify the evolved product gases (representative raw chronoamperograms and GC traces are shown in the SI, **Figures S11-S12**). For AuPTFE, at −0.80 V (all potentials are reported relative to the reversible hydrogen electrode at pH 6.8; see **SI Methods** for further details), we observe a CO partial geometric current density (j_{CO}) of 2.7 mA cm^{-2} (**Figure 2a**, left plot, yellow points) corresponding to 95% faradaic efficiency (FE) (**Figure 2a**, right plot, yellow points), with a H_2 partial geometric current density (j_{H2}) of 0.2 mA cm^{-2} accounting for the balance current density and FE. At a more negative potential of −1.16 V, CO_2RR and HER current densities rise to 6.7 mA cm^{-2} and 0.9 mA cm^{-2}, respectively, with a monotonic increase between these potentials. Over the entire potential range canvassed, the FE for CO_2RR remained roughly unchanged between 90 and 95 percent (**Figure 2**, right), with the remainder of the faradaic balance accounted for by H_2. AgPTFE also displays high selectivity for CO production in 0.1 M $NaHCO_3$ electrolyte. At −0.82 V, AgPTFE displays a j_{CO} of 0.5 mA cm^{-2} (**Figure 2b**, left, yellow points) and a j_{H2} of 0.06 mA cm^{-2} (**Figure 2b**, left plot, blue points), giving a CO:H_2 FE ratio of 91:9. The CO partial current density increases to 4.7 mA cm^{-2} at a more negative applied potential of −1.20 V with a corresponding increase in j_{H2} of 0.2 mA cm^{-2}. Across this potential range, the FE for CO_2RR remains roughly constant between 91-96% (**Figure 2b**, right). The high observed selectivity for CO on AuPTFE

and AgPTFE in our hands is in line with literature reports of CO_2RR on both metals.[37,38]
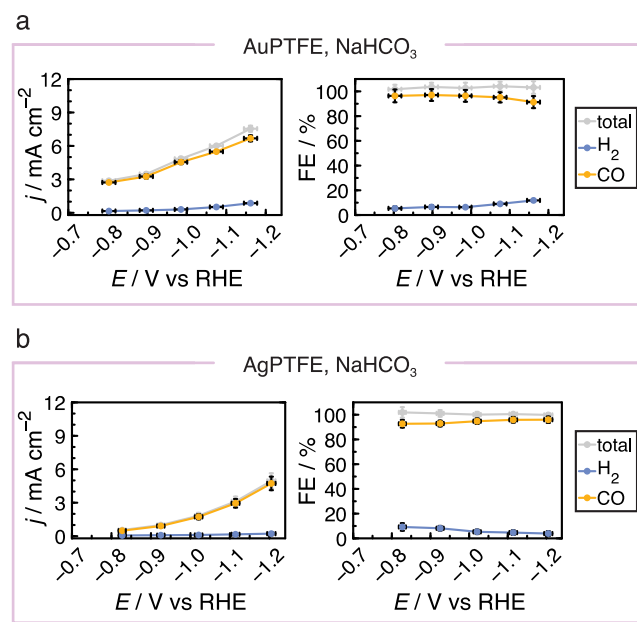
Figure 2. a, Partial geometric current densities (left), and faradaic efficiencies (right) for AuPTFE-catalyzed CO_2RR and HER in 0.1 M $NaHCO_3$ for a range of potentials. **b**, Partial geometric current densities (left), and faradaic efficiencies (right) for AgPTFE-catalyzed CO_2RR and HER in 0.1 M $NaHCO_3$. All values are the mean of three or more measurements, and error bars represent the standard error of three or more separate electrode and cell setups. Error bars that are not visible are smaller than the data point marker.

Having established the baseline activity of AuPTFE and AgPTFE in $NaHCO_3$ electrolyte we next investigated CO_2RR activity and selectivity in the presence of a tetraalkylammonium bicarbonate electrolyte. As a starting point for these studies, tetraethylammonium (TEA$^+$) was chosen because its ethyl groups inhibit direct Lewis acid-base coordination[34] and it is commercially available as an electrochemical-grade aqueous solution. $TEAHCO_3$ electrolyte was prepared by acidifying a stock solution of electrochemical-grade tetraethylammonium hydroxide (TEAOH) with CO_2 until the pH of the solution became neutral (see **SI Methods** for further details). For a AuPTFE electrode polarized to −0.75 V in 0.1 M $TEAHCO_3$, (pH 6.9) we observe a j_{CO} of 1.6 mA cm^{-2} and j_{H2} of 0.6 mA cm^{-2} (**Figure 3a**, left). This corresponds to a 40% decrease in j_{CO} and a four-fold increase in j_{H2} relative to the performance of AuPTFE in 0.1 M $NaHCO_3$ at the same applied potential. Upon polarization to more negative potentials, both CO and H_2 partial currents increase monotonically, up to a j_{CO} of 4.9 mA cm^{-2} and j_{H2} of 1.8 mA cm^{-2} at −1.12 V, corresponding to a 27% decrease in j_{CO} and a two-fold increase in j_{H2} compared to $NaHCO_3$. Across the range of potentials probed, the CO:H_2 FE ratio remained roughly constant at 70:30 (**Figure 3a**, right) in favor of CO.

To see if this change in activity between $NaHCO_3$ and $TEAHCO_3$ electrolytes is conserved for different catalyst materials, we next investigated the CO_2 reduction ability of

AgPTFE in 0.1 M TEAHCO₃ electrolyte. At −0.80 V, the performance of AgPTFE in 0.1 M TEAHCO₃ matches that of its performance in 0.1 M NaHCO₃, with a j_{CO} of 0.5 mA cm⁻² and j_{H2} of 0.08 mA cm⁻² (**Figure 2b**, left). However, at more negative potentials, j_{CO} in TEAHCO₃ only reaches 3.0 mA cm⁻² at −1.20 V, corresponding to a 36% decrease relative to NaHCO₃. j_{H2} at more negative potentials is comparable for both NaHCO3 and TEAHCO₃ electrolytes, reaching 0.2 mA cm⁻² at −1.20 V. Across this potential range, the FE for CO fluctuated between 95 and 89 percent with the balance accounted for by H₂ (**Figure 2b**, right). Although the rates of Au- and Ag-catalyzed CO₂RR in TEAHCO₃ electrolyte are diminished relative to NaHCO₃ electrolyte, we were intrigued by the observation of substantial CO production in this non-conventional electrolyte.


a

AuPTFE, TEAHCO₃

b

AgPTFE, TEAHCO₃
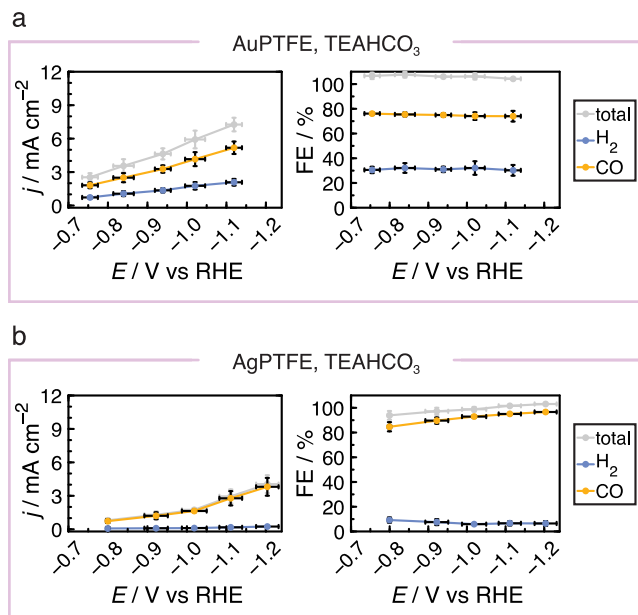
Figure 3. a, Partial geometric current densities (left), and faradaic efficiencies (right) for AuPTFE-catalyzed CO₂RR and HER in 0.1 M TEAHCO₃ for a range of potentials. **b**, Partial geometric current densities (left), and faradaic efficiencies (right) for AgPTFE-catalyzed CO₂RR and HER in 0.1 M TEAHCO₃. All values are the mean of three or more measurements, and error bars represent the standard error of three or more separate electrode and cell setups. Error bars that are not visible are smaller than the data point marker.

As highlighted above, trace alkali metal cations are common in aqueous electrochemical cells. To determine whether our results were affected by adventitious alkali metal contaminants, we quantified the levels of alkali metal cations in our TEAHCO₃ electrolyte before and after electrolysis by ICP-MS (**Tables S3-S4**). We found that Na⁺ was the most abundant alkali metal cation contaminant in our 100 mM TEA⁺ electrolyte, present at 7 ± 4 μM. Consequently, in a typical experiment in 100 mM TEA⁺, the weakly-coordinating organic cations exceed alkali metal cations by four orders of magnitude. Despite the large excess of TEA⁺ relative to Na⁺, we acknowledge that the trace population of alkali cation could play an outsized role in dictating the catalytic activity of the interface. To probe the extent to which trace alkali

cations are contributing to the observed CO₂RR activity, we prepared a series of binary electrolyte mixtures ranging from the native TEAHCO₃ electrolyte with a Na⁺ mole fraction (χ_{Na+}) of 10⁻⁴ to a pure NaHCO₃ electrolyte (χ_{Na+} of 1), keeping the total ionic strength constant at 100 mM. Using AuPTFE as the working electrode, we quantified catalytic activity across this electrolyte series at a constant applied potential of −0.95 V. Varying χ_{Na+} from 10⁻⁴ to 10⁻³ leads to a 5% increase in faradaic efficiency in favor of CO₂RR, with another 5% increase in CO₂RR occurring as χ_{Na+} increases to 10⁻² and the corresponding decrease in HER faradaic efficiency that preserves the total faradaic balance close to 100% (**Figure 4**). The largest change in selectivity as a function of electrolyte condition occurs between χ_{Na+} of 10⁻² and 0.1, in which CO₂RR faradaic efficiency increases from 75% to 90%. Continuing to increase χ_{Na+} up to 0.2 completes the smooth transition in selectivity towards the selectivity in bulk NaHCO₃. Although the activity trend appears to asymptote at low χ_{Na+}, the data suggest that for χ_{Na+} between 10⁻⁴ and 0.1, (**Figure 4**, purple region), the catalytic activity is influenced by the presence of both Na⁺ and TEA⁺ at the interface. Furthermore, this observation emphasizes that in order to study the intrinsic effects of organic cations on the CO₂RR, the introduction of alkali metal cation-containing electrolytes should be avoided, as the presence of as little as 1 mM Na⁺ may convolute measurements of catalytic activity.

As χ_{Na+} is increased beyond 0.2, both CO₂RR selectivity and rate remain unchanged and matches the values observed for pure 0.1 M NaHCO₃ electrolyte (**Figure 2a**), suggesting that the interface becomes saturated in Na⁺ once χ_{Na+} reaches 0.2 (**Figure 4**, pink region). The implications of this result are two-fold. First, this observation suggests that the surface affinity of Na⁺ is much higher than TEA⁺, causing it to outcompete TEA⁺ at the interface even when TEA⁺ is in vast excess. Additionally, this observation suggests that, despite the presence of less than 10⁻⁴ mole fraction of Na⁺ in the as-prepared 100 mM TEAHCO₃, the catalytic activity deviates substantially from that in pure Na⁺, indicating that the data above in **Figure 2** is at least partially reflective of CO₂RR activity facilitated by interfacial TEA⁺. However, in this electrolyte, we do not observe a clear plateau in activity across a range of χ_{Na+} conditions, preventing us from unequivocally excluding some influence from trace Na⁺ accumulated at the interface.
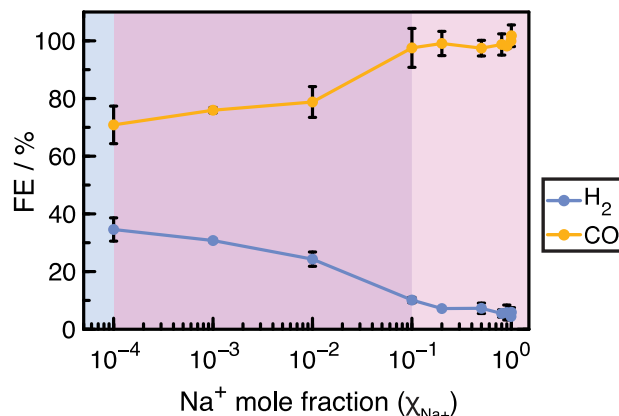
Figure 4. Changes in CO and H_2 faradaic efficiency for AuPTFE at -0.95 V as Na^+ mole fraction (χ_{Na^+}) is varied from ca. 10^{-4} to 1 in a binary supporting electrolyte of $TEAHCO_3$ and $NaHCO_3$, keeping the total ionic strength constant at 0.1 M. The region highlighted in blue is the region in which catalytic activity matches that of AuPTFE in 0.1 M $TEAHCO_3$. The region highlighted in purple is the transition region, in which both Na^+ and TEA^+ affect interfacial reactivity. The region highlighted in pink is the region in which catalytic activity matches that of AuPTFE in 0.1 M $NaHCO_3$. All values are the mean of three measurements. Error bars represent the standard error of three or more measurements with separate cell setups. Error bars that are not visible are smaller than the data point marker. For plots of partial geometric current densities as a function of electrolyte cation composition, see **Figure S27**.

To address the foregoing ambiguity, we examined a tetraalkylammonium polyelectrolyte. Since polyelectrolytes can be purified using size exclusion methods, we hypothesized that that these electrolytes could be purified of Na^+ contaminants more rigorously than electrolytes based on small-molecule organic cations such as TEA^+. Additionally, polyelectrolytes may have vastly differential surface affinity relative to a small ion such as Na^+, providing a greater tolerance for the latter. Poly(dimethyl diallyl ammonium) ($pDDA^+$, M_w = 400,000-500,000 Da), a commercially available water-soluble polymer, was chosen as a model polyelectrolyte cation. As obtained, this polymer has tetraalkylammonium repeat units bearing chloride counter-anions. To generate an equivalent comparison with traditional carbonate electrolytes, we dialyzed the chloride form of $pDDA^+$ with $(NH_4)_2CO_3$, affording the corresponding polyelectrolyte carbonate buffer. Residual $(NH_4)_2CO_3$ was removed by exhaustive dialysis against MilliQ water (full details of the dialysis, purification, and characterization of $pDDAHCO_3$ are included in the **SI Methods** section and **Figures S9-S10**). ICP-MS quantification of our polyelectrolyte immediately after dialysis shows only low micromolar quantities of alkali metal contaminants (2 ± 2 for a 500 mM stock solution of $pDDAHCO_3$), significantly lower than that of commercial TEAOH (**Table S3**). Thus, in a typical experiment with 0.1 M $pDDA^+$, the $pDDA^+$ concentration exceeds that of trace alkali metal cations by at least five orders of magnitude.

To investigate whether this electrolyte could support the CO_2RR at comparable rates to previously investigated electrolytes, we polarized AuPTFE working electrodes in 0.1 M $pDDAHCO_3$ (pH 6.8) and quantified the evolved products by gas chromatography. In $pDDAHCO_3$ electrolyte, AuPTFE produced a mixture of CO and H_2. At -0.74 V in $pDDAHCO_3$, we measured a j_{CO} of 2.6 mA cm^{-2}, a rate comparable to that of j_{CO} in $NaHCO_3$ of 2.7 mA cm^{-2}. The rate of AuPTFE-catalyzed CO production increases at more negative potentials—albeit at a slower rate relative to other electrolytes, reaching 4.2 mA cm^{-2} at -1.07 V (**Figure 5a**, yellow points). In the most extreme case, this corresponds to a 37% decrease in j_{CO} relative to that in $NaHCO_3$ (**Figure 2a**). Most strikingly, in $pDDAHCO_3$ electrolyte, Au-catalyzed HER is enhanced significantly relative to $NaHCO_3$ (**Figure 5a**, blue points). At -0.74 V, j_{H2} is 0.9 mA cm^{-2}, corresponding to a nearly five-fold increase relative to j_{H2} in $NaHCO_3$. The rate of HER increased faster than that of CO_2RR across this

potential range, eventually outcompeting the rate of CO_2RR at a point between -0.91 and -0.99 V. Consequently, the FE for H_2 production increased over this potential range, beginning at 25% at -0.75 V and reaching 64% at -1.07 V (**Figure 5b**). Similar to our observations in $TEAHCO_3$ electrolyte, use of $pDDAHCO_3$ electrolyte leads to an attenuation in CO production rate and faradaic efficiency relative to $NaHCO_3$ but nevertheless, this organic polycation is still able to support substantial CO_2RR activity.

We next examined CO_2RR on AgPTFE in $pDDAHCO_3$ electrolyte. Across the entire range of potentials tested the CO faradaic efficiency was between 98 to 100% (**Figure 5d**, yellow points). These faradaic efficiency values are comparable to what we measured for AgPTFE in $NaHCO_3$ electrolyte (**Figure 2c**). To our surprise, we observed a j_{CO} of 2.1 mA cm^{-2} in $pDDAHCO_3$ electrolyte at -0.76 V, corresponding to a 4.3-fold increase relative to $NaHCO_3$. CO partial current density increased monotonically from -0.76 to -1.10 V, reaching 8.9 mA cm^{-2} at -1.10 V (**Figure 5b**, yellow points), corresponding to a nearly two-fold increase in j_{CO} relative to $NaHCO_3$. Across this entire range, H_2 production was low, beginning at 0.03 mA cm^{-2} at -0.76 V and reaching a maximum of only 0.1 mA cm^{-2} at -1.10 V. The enhancement of CO production rate and retention of high CO selectivity for AgPTFE (**Figure 5b**) is at odds with the slight attenuation in rate and CO selectivity for AuPTFE (**Figure 5a**). While the precise origin of this divergent selectivity trend remains unclear, the high activity and selectivity for CO_2RR on AgPTFE in $pDDAHCO_3$ suggests that organic cations are viable electrolytes for CO_2-to-fuels conversion.

a

AuPTFE, $pDDAHCO_3$

b

AgPTFE, $pDDAHCO_3$
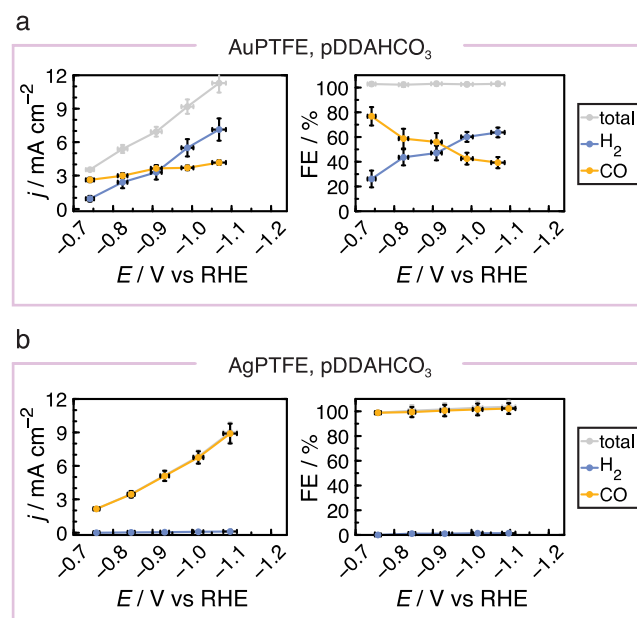
Figure 5. a, Partial geometric current densities (left), and faradaic efficiencies (right) for AuPTFE-catalyzed CO_2RR and HER in 0.1 M $pDDAHCO_3$ for a range of potentials. **b**, Partial geometric current densities (left), and faradaic efficiencies (right) for AgPTFE-catalyzed CO_2RR and HER in 0.1 M $pDDAHCO_3$. All values are the mean of three or more measurements, and error bars represent the standard error of three or more separate electrode and cell setups. Error bars that are not visible are smaller than the data point marker.

As highlighted above, pDDAHCO$_3$ was chosen as an example electrolyte because it could be purified by dialysis to low micromolar levels of alkali metal impurities; however, even with all precautions taken to remove alkali metal contaminants, we still observed ca. 1 μM adventitious Na$^+$ in our working compartment electrolyte by post-mortem ICP-MS analysis (**Table S4**). To determine whether this trace alkali metal cation population is contributing to the observed CO$_2$RR activity, we repeated the same competition experiment above (**Figure 4**) with AuPTFE and varying ratios of pDDA$^+$ and Na$^+$. At −0.95 V, we observe that between a Na$^+$ mole fraction, χ_{Na+}, of 10^{-5} and 0.5, the catalytic activity of Au in 0.1 M pDDAHCO$_3$ was largely unchanged, with CO accounting for between 56 and 61% of the overall FE (**Figure 6**, blue region). This observation is in stark contrast with our observation of a systematic increase in CO selectivity over the same mole fraction range in Na$^+$/TEA$^+$ binary electrolytes (**Figure 4**). We ascribe the constancy in CO/H$_2$ selectivity over the nominal range from 100% pDDA$^+$ (χ_{Na+} = 10^{-5}) to 50% pDDA$^+$ (χ_{Na+} = 0.5) to an interfacial reaction environment that is fully saturated with pDDA$^+$ ions such that the electrocatalytic selectivity is dictated predominantly by pDDA$^+$ with negligible contribution from Na$^+$ (**Figure 6**, blue region). For the χ_{Na+} range between 0.5 and 0.8, we observed a 3% increase in CO selectivity suggesting that Na$^+$ may be playing a minor contributing role over this range. However, we observe the largest changes in catalytic activity for electrolytes with χ_{Na+} above 0.8. Indeed, between χ_{Na+} of 0.9 and 0.99, we observed a 17% increase in CO faradaic efficiency, at the expense of H$_2$ production (**Figure 6**, purple region, highlighted in the top left inset). In this Na$^+$ rich region, the smooth transition between the intrinsic selectivity of AuPTFE implies that catalytic activity is influenced by a combination of Na$^+$ and pDDA$^+$ at the interface. Critically, this analysis reveals that all previous experiments conducted in 0.1 M pDDAHCO$_3$ electrolyte (**Figure 5**) fall within the regime in which pDDA$^+$ dominates catalytic activity (**Figure 6**, blue region). Thus, these competition experiments bolster the notion that the data in **Figure 5** samples the intrinsic ability of pDDA$^+$ cations to foster CO$_2$ reduction catalysis.

The observation that catalysis in pDDAHCO$_3$ electrolyte is remarkably insensitive to Na$^+$ addition up to a χ_{Na+} of 0.8 suggests that pDDA$^+$ preferentially migrates and/or adsorbs to the interface under reductive polarization. A polymeric electrolyte such as pDDA$^+$ may also reversibly form a thin film on the electrode surface, effectively rejecting Na$^+$ ion transport to the surface. The formation of organic films—both in situ[22] and ex situ[29]—have been well-documented in the CO$_2$RR literature; however, we emphasize that all of these studies involved additives that are only sparingly soluble or completely insoluble in water. In contrast, the use of a fully water-soluble (poly)cations in this study permitted studies across a wide range of bulk concentration ratios. While we uncover a clear ratio-independent regime for the pDDA$^+$/Na$^+$ binary system, a similar regime may not exist for all cations, emphasizing the importance of cation competition experiments for probing the interfacial cation micro-environment persistent under CO$_2$RR conditions.
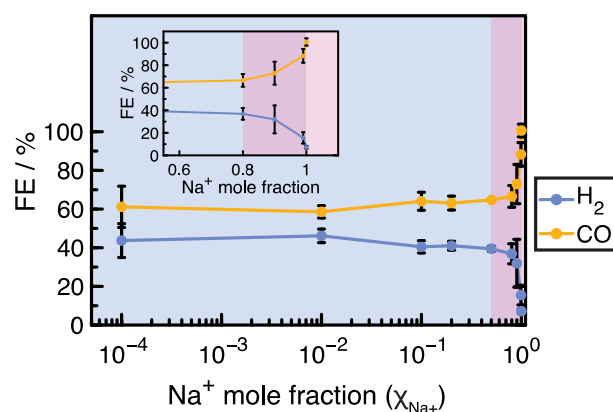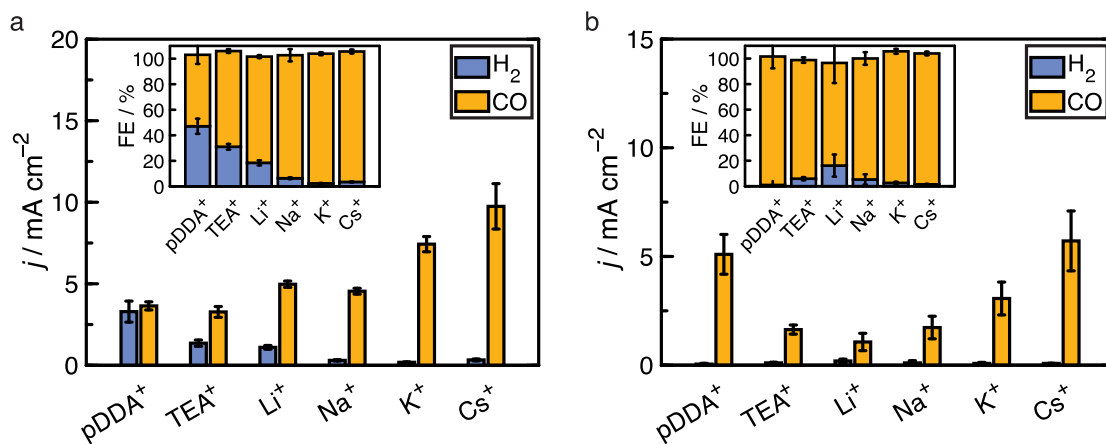

Figure 6. a, Changes in CO and H$_2$ faradaic efficiency for AuPTFE at −0.95 V as Na$^+$ mole fraction (χ_{Na+}) is varied from ca. 10^{-5} to 1 in a binary supporting electrolyte of pDDAHCO$_3$ and NaHCO$_3$, keeping the total ionic strength constant at 0.1 M. The region highlighted in blue is the region in which catalytic activity matches that of AuPTFE in 0.1 M pDDAHCO$_3$. The region highlighted in purple is the transition region, in which both Na$^+$ and pDDA$^+$ affect interfacial reactivity. The region highlighted in pink is the region in which catalytic activity matches that of AuPTFE in 0.1 M NaHCO$_3$. Inset: zoom in of the transition region in which a smooth change in catalytic activity is observed. All values are the mean of three measurements. Error bars represent the standard error of three or more measurements with separate cell setups. Error bars that are not visible are smaller than the data point marker. For plots of partial current densities as a function of electrolyte cation composition, see **Figure S28**.

Catalytic trends between organic and alkali cations suggest that coordination plays a minor role in CO$_2$ activation.

Using the above methodology, we compared the aqueous CO$_2$ reduction performance of AuPTFE in 0.1 M bicarbonate electrolytes containing TEA$^+$ and pDDA$^+$ with the performance of the same material in electrolytes containing the typically studied alkali metal cations: Li$^+$, Na$^+$, K$^+$, and Cs$^+$. At −0.97 V (see SI for full data sets for each of these electrolytes over a range of potentials and a plot of these data sets overlaid with each other, **Figures S15-S20**; **Figure S29a**), AuPTFE displays a roughly two-fold increase in j_{CO} across the alkali metal cation series spanning 4.9 and 4.5 mA cm^{-2} in LiHCO$_3$ and NaHCO$_3$ to 10.2 mA cm^{-2} in CsHCO$_3$ (**Figure 7a**, yellow bars), with a concomitant decrease in j_{H2} across the same series (**Figure 7a**, blue bars). These changes as a function of electrolyte cation identity are reflected in the faradaic efficiencies for CO and H$_2$, with the CO faradaic efficiency being the lowest in LiHCO$_3$ at 82% and the highest in CsHCO$_3$ at 97% (**Figure 7a**, inset). This trend in rate and selectivity for the CO$_2$RR is consistent with literature reports.[15] At the same potential in TEA$^+$ electrolyte, we observed a j_{CO} of 3 mA cm^{-2} (**Figure 7a**), corresponding to a 40% decrease in j_{CO} compared to Li$^+$, the alkali metal cation with the lowest j_{CO} of the series. In pDDA$^+$ electrolyte, we observed a j_{CO} of 3.6 mA cm^{-2} (**Figure 7a**), comparable to

that in TEA⁺. In both TEA⁺ and pDDA⁺ electrolytes, the rate and selectivity for HER was increased relative to the alkali metal bicarbonate electrolytes (**Figure 7a**, inset). While a full examination of these trends is beyond the scope of this study, we note that the j_{CO} for both organic cations is roughly in line with what would be expected based on their hydrated ion radius[39], a descriptor that has been used to rationalize trends across alkali metal cations[15]. Irrespective of the specific reasons, we stress that the difference in j_{CO} across this series of organic and alkali metal cations fall well within the range reported previously for alkali cation series alone, emphasizing that tetraalkylammonium cations are competent for supporting CO₂RR catalysis despite their weakly coordinating nature.

The above trends for AuPTFE are not held for AgPTFE. For Ag, at −0.94 V (see SI for full data sets for each of these electrolytes over a range of potentials and a plot of these data sets overlaid with each other, **Figures S21-S26**; **Figure S29b**), we observe a nearly six-fold increase in j_{CO} across the alkali metal cation series from 1.0 mA cm⁻² in LiHCO₃ to 5.7 mA cm⁻² in CsHCO₃ (**Figure 7b**, yellow bars), corresponding to faradaic efficiencies of 82 and 101%, respectively

(**Figure 7b**, inset). Although consistently low across the entire series, j_{H2} decreased from 0.2 mA cm⁻² in LiHCO₃ to 0.08 mA cm⁻² in CsHCO₃ across this series (**Figure 7b**, yellow bars), corresponding to faradaic efficiencies of 16 and 1%, respectively (**Figure 7b**, inest). These trends are in line with the trends observed on AuPTFE: that is, j_{CO} increases going down the periodic table. However, unlike for AuPTFE, the performance of AgPTFE in electrolytes with organic cations is contrary to expectations based on hydrated ion size. For AgPTFE, we found a j_{CO} of 1.6 mA cm⁻², corresponding to a three-fold increase in CO partial current density relative to Li⁺ electrolyte. Even more striking is the observation that AgPTFE-catalyzed CO₂ reduction in pDDAHCO₃ proceeded with a j_{CO} of 5.1 mA cm⁻² (**Figure 7b**), comparable to the most promoting alkali ion, Cs⁺. Whereas activity/selectivity trends across alkali cations are generally conserved across metal surfaces, the foregoing observations suggest that this is not the case for organic cations, opening the door to designer pairings of cations and electrocatalysts for selective CO₂RR.

Figure 7. a, Steady-state partial geometric current densities and faradaic efficiencies (inset) for AuPTFE-catalyzed CO₂RR and HER at −0. 97 V in bicarbonate electrolytes with varying cations. **b**, Steady-state partial geometric current densities and faradaic efficiencies (inset) for AgPTFE-catalyzed CO₂RR and HER at −0. 94 V in bicarbonate electrolytes with varying cations. All values are the mean of three or more measurements in separate cells. Error bars represent the standard error of three or more measurements with separate cell setups. Error bars that are not visible are smaller than the data point marker.

CONCLUSION

Understanding the origins of cation effects is critical for developing electrolyte design principles for next-generation CO₂ reduction technologies. To this end, we developed a methodology for determining the intrinsic ability of organic cations to foster CO₂ reduction. Specifically, catalytic trends across a series of binary mixtures of organic and alkali ion electrolytes exposed regimes in which catalysis was dictated by the organic cation identity, alkali metal cation identity, or a mixture of the two (**Figure 4**, **Figure 6**). Working in the regime in which catalysis is controlled by an organic polyelectrolyte cation, pDDA⁺, we find that weakly-coordinating organic cations are intrinsically capable of fostering Au- and Ag-catalyzed CO₂ reduction to CO.

For Au-catalyzed CO₂RR, TEA⁺ and pDDA⁺ electrolytes give to CO₂ reduction activities that are comparable to Li⁺ and Na⁺ electrolytes, but with diminished selectivity due to enhanced H₂ evolution rates (**Figure 7a**). In contrast, for Ag-

catalyzed CO₂RR, CO₂ reduction activities are comparable to Cs⁺ electrolytes with retention of high selectivity (**Figure 7b**). Importantly, across all data collected, rates of CO₂ reduction in alkali metal bicarbonate and tetraalkylammonium bicarbonate electrolytes are within one order of magnitude, suggesting that specific coordination to reaction intermediates plays a minor role in facilitating CO₂ reduction to CO. In aggregate, these findings support a revision of electrolyte design principles. Unlike metal cations, organic cations are synthetically tunable, substantially expanding the structure space available for electrolyte design. The methodology set forward here allows for detailed mechanistic investigations of electrolyte cation structure-function correlations in CO₂RR catalysis in this largely unexplored design space.

ASSOCIATED CONTENT

Supporting Information

The Supporting Information is available free of charge on the ACS Publications website.

AUTHOR INFORMATION

Corresponding Author

* Yogesh Surendranath – Department of Chemistry, Massachusetts Institute of Technology, Cambridge, Massachusetts 02139, United States; orcid.org/0000-0003-1016-3420; Email: yogi@mit.edu

Authors

Sophia Weng – Department of Chemistry, Massachusetts Institute of Technology, Cambridge, Massachusetts, 02139, United States; orcid.org/0000-0002-9055-1732

Wei Lun Toh – Department of Chemistry, Massachusetts Institute of Technology, Cambridge, Massachusetts, 02139, United States; orcid.org/0000-0001-9001-0488

REFERENCES

(1) Nitopi, S.; Bertheussen, E.; Scott, S. B.; Liu, X.; Engstfeld, A. K.; Horch, S.; Seger, B.; Stephens, I. E. L.; Chan, K.; Hahn, C.; et al. Progress and Perspectives of Electrochemical CO₂ Reduction on Copper in Aqueous Electrolyte. *Chem. Rev.* **2019**, *119* (12), 7610–7672.

(2) Marcandalli, G.; Monteiro, M. C. O.; Goyal, A.; Koper, M. T. M. Electrolyte Effects on CO₂ Electrochemical Reduction to CO. *Acc. Chem. Res.* **2022**, *55* (14), 1900–1911.

(3) Wuttig, A.; Yaguchi, M.; Motobayashi, K.; Osawa, M.; Surendranath, Y. Inhibited Proton Transfer Enhances Au-Catalyzed CO₂-to-Fuels Selectivity. *Proc. Natl. Acad. Sci. U. S. A.* **2016**, *113* (32), E4585–E4593.

(4) Murata, A.; Hori, Y. Product Selectivity Affected by Cationic Species in Electrochemical Reduction of CO₂ and CO at a Cu Electrode. *Bull. Chem. Soc. Jpn.* **1991**, *64* (1), 123–127.

(5) Xu, A.; Govindarajan, N.; Kastlunger, G.; Vijay, S.; Chan, K. Theories for Electrolyte Effects in CO₂ Electroreduction. *Acc. Chem. Res.* **2022**, *55* (4), 495–503.

(6) Waegele, M. M.; Gunathunge, C. M.; Li, J.; Li, X. How Cations Affect the Electric Double Layer and the Rates and Selectivity of Electrocatalytic Processes. *J. Chem. Phys.* **2019**, *151* (16), 160902.

(7) Marcandalli, G.; Goyal, A.; Koper, M. T. M. Electrolyte Effects on the Faradaic Efficiency of CO₂ Reduction to CO on a Gold Electrode. *ACS Catal.* **2021**, *11* (9), 4936–4945.

(8) Singh, M. R.; Kwon, Y.; Lum, Y.; Ager, J. W.; Bell, A. T. Hydrolysis of Electrolyte Cations Enhances the Electrochemical Reduction of CO₂ over Ag and Cu. *J. Am. Chem. Soc.* **2016**, *138* (39), 13006–13012.

(9) Resasco, J.; Chen, L. D.; Clark, E.; Tsai, C.; Hahn, C.; Jaramillo, T. F.; Chan, K.; Bell, A. T. Promoter Effects of Alkali Metal Cations on the Electrochemical Reduction of Carbon Dioxide. *J. Am. Chem. Soc.* **2017**, *139* (32), 11277–11287.

(10) Dattila, F.; Monteiro, M. C. O.; Koper, M. T. M.; López, N. Reply to: On the Role of Metal Cations in CO₂ Electrocatalytic Reduction. *Nat. Catal.* **2022**, *5* (11), 979–981.

(11) Shin, S. J.; Choi, H.; Ringe, S.; Won, D. H.; Oh, H. S.; Kim, D. H.; Lee, T.; Nam, D. H.; Kim, H.; Choi, C. H. A Unifying Mechanism for Cation Effect Modulating C1 and C2 Productions from CO₂ Electroreduction. *Nat. Commun.* **2022**, *13* (1), 1–10.

(12) Qin, X.; Vegge, T.; Hansen, H. A. Cation-Coordinated Inner-Sphere CO₂ Electroreduction at Au-Water Interfaces. *J. Am. Chem. Soc.* **2023**, *145* (3), 1897–1905.

(13) Ayemoba, O.; Cuesta, A. Spectroscopic Evidence of Size-Dependent Buffering of Interfacial pH by Cation Hydrolysis during CO₂ Electroreduction. *ACS Appl. Mater. Interfaces* **2017**, *9* (33), 27377–27382.

(14) Malkani, A. S.; Anibal, J.; Xu, B. Cation Effect on Interfacial CO₂ Concentration in the Electrochemical CO₂ Reduction Reaction. *ACS Catal.* **2020**, *10* (24), 14871–14876.

(15) Ringe, S.; Clark, E. L.; Resasco, J.; Walton, A.; Seger, B.; Bell, A. T.; Chan, K. Understanding Cation Effects in Electrochemical CO₂ Reduction. *Energy Environ. Sci.* **2019**, *12* (10), 3001–3014.

(16) Chen, L. D.; Urushihara, M.; Chan, K.; Nørskov, J. K. Electric Field Effects in Electrochemical CO₂ Reduction. *ACS Catal.* **2016**, *6* (10), 7133–7139.

(17) Ovalle, V. J.; Hsu, Y. S.; Agrawal, N.; Janik, M. J.; Waegele, M. M. Correlating Hydration Free Energy and Specific Adsorption of Alkali Metal Cations during CO₂ Electroreduction on Au. *Nat. Catal.* **2022**, *5* (7), 624–632.

(18) Gu, J.; Liu, S.; Ni, W.; Ren, W.; Haussener, S.; Hu, X. Modulating Electric Field Distribution by Alkali Cations for CO₂ Electroreduction in Strongly Acidic Medium. *Nat. Catal.* **2022**, *5* (4), 268–276.

(19) Monteiro, M. C. O.; Dattila, F.; Hagedoorn, B.; García-Muelas, R.; López, N.; Koper, M. T. M. Absence of CO₂ Electroreduction on Copper, Gold and Silver Electrodes without Metal Cations in Solution. *Nat. Catal.* **2021**, *4* (8), 654–662.

(20) Le, D.; Rahman, T. S. On the Role of Metal Cations in CO₂ Electrocatalytic Reduction. *Nat. Catal.* **2022**, *5* (11), 977–978.

(21) Monteiro, M. C. O.; Dattila, F.; López, N.; Koper, M. T. M. The Role of Cation Acidity on the Competition between Hydrogen Evolution and CO₂ Reduction on Gold Electrodes. *J. Am. Chem. Soc.* **2022**, *144* (4), 1589–1602.

(22) Banerjee, S.; Gerke, C. S.; Thoi, V. S. Guiding CO₂RR Selectivity by Compositional Tuning in the Electrochemical Double Layer. *Acc. Chem. Res.* **2022**, *55* (4), 504–515.

(23) Quan, F.; Xiong, M.; Jia, F.; Zhang, L. Efficient Electroreduction of CO₂ on Bulk Silver Electrode in Aqueous Solution via the Inhibition of Hydrogen Evolution. *Appl. Surf. Sci.* **2017**, *399*, 48–54.

(24) Kim, C.; Bui, J. C.; Luo, X.; Cooper, J. K.; Kusoglu, A.; Weber, A. Z.; Bell, A. T. Tailored Catalyst Microenvironments for CO₂ Electroreduction to Multicarbon Products on Copper Using Bilayer Ionomer Coatings. *Nat. Energy* **2021**, *6* (11), 1026–1034.

(25) Nie, W.; Heim, G. P.; Watkins, N. B.; Agapie, T.; Peters, J. C. Organic Additive-Derived Films on Cu Electrodes Promote Electrochemical CO₂ Reduction to C2⁺ Products Under Strongly Acidic Conditions. *Angew. Chemie Int. Ed.* **2023**, *62* (12), e202216102.

(26) Thevenon, A.; Rosas-Hernández, A.; Fontani Herreros, A. M.; Agapie, T.; Peters, J. C. Dramatic HER Suppression on Ag Electrodes via Molecular Films for Highly Selective CO₂ to CO Reduction. *ACS Catal.* **2021**, *11* (8), 4530–4537.

(27) Ozden, A.; Li, F.; García De Arquer, F. P.; Rosas-Hernández, A.; Thevenon, A.; Wang, Y.; Hung, S. F.; Wang, X.; Chen, B.; Li, J.; et al. High-Rate and Efficient Ethylene Electrosynthesis Using a Catalyst/Promoter/Transport Layer. *ACS Energy Lett.* **2020**, *5* (9), 2811–2818.

(28) Lai, Y.; Watkins, N. B.; Rosas-Hernández, A.; Thevenon, A.; Heim, G. P.; Zhou, L.; Wu, Y.; Peters, J. C.; Gregoire, J. M.; Agapie, T. Breaking Scaling Relationships in CO_2 Reduction on Copper Alloys with Organic Additives. *ACS Cent. Sci.* **2021**, *7* (10), 1756–1762.

(29) Buckley, A. K.; Cheng, T.; Oh, M. H.; Su, G. M.; Garrison, J.; Utan, S. W.; Zhu, C.; Toste, F. D.; Goddard, W. A.; Toma, F. M. Approaching 100% Selectivity at Low Potential on Ag for Electrochemical CO_2 Reduction to CO Using a Surface Additive. *ACS Catal.* **2021**, *11* (15), 9034–9042.

(30) Koshy, D. M.; Akhade, S. A.; Shugar, A.; Abiose, K.; Shi, J.; Liang, S.; Oakdale, J. S.; Weitzner, S. E.; Varley, J. B.; Duoss, E. B.; et al. Chemical Modifications of Ag Catalyst Surfaces with Imidazolium Ionomers Modulate H_2 Evolution Rates during Electrochemical CO_2 Reduction. *J. Am. Chem. Soc.* **2021**, *143* (36), 14712–14725.

(31) Fan, L.; Liu, C. Y.; Zhu, P.; Xia, C.; Zhang, X.; Wu, Z. Y.; Lu, Y.; Senftle, T. P.; Wang, H. Proton Sponge Promotion of Electrochemical CO_2 Reduction to Multi-Carbon Products. *Joule* **2022**, *6* (1), 205–220.

(32) Qin, H.-G.; Du, Y.-F.; Bai, Y.-Y.; Li, F.-Z.; Wang, H.; Peng, J.-Z.; Gu, J. Surface-Immobilized Cross-Linked Cationic Polyelectrolyte Enables CO_2 Reduction with Metal Cation-Free Acidic Electrolyte. **2023**, Research Square preprint.

(33) Bondue, C. J.; Graf, M.; Goyal, A.; Koper, M. T. M. Suppression of Hydrogen Evolution in Acidic Electrolytes by Electrochemical CO_2 Reduction. *J. Am. Chem. Soc.* **2021**, *143* (1), 279–285.

(34) Ueno, K.; Tokuda, H.; Watanabe, M. Ionicity in Ionic Liquids: Correlation with Ionic Structure and Physicochemical Properties. *Phys. Chem. Chem. Phys.* **2010**, *12* (8), 1649–1658.

(35) Hori, Y.; Murata, A.; Kikuchi, K.; Suzuki, S. Electrochemical Reduction of Carbon Dioxide to Carbon Monoxide at a Gold Electrode in Aqueous Potassium Hydrogen Carbonate. *J. Chem. Soc., Chem. Commun.* **1987**, 728-729.

(36) Hori, Y.; Kikuchi, K.; Suzuki, S. Production of CO and CH_4 in electrochemical reduction of CO_2 at metal electrodes in aqueous hydrogencarbonate solution. *Chem. Lett.* **1985**, *14* (11), 1695–1698.

(37) Goyal, A.; Marcandalli, G.; Mints, V. A.; Koper, M. T. M. Competition between CO_2 Reduction and Hydrogen Evolution on a Gold Electrode under Well-Defined Mass Transport Conditions. *J. Am. Chem. Soc.* **2020**, *142* (9), 4154–4161.

(38) Clark, E. L.; Bell, A. T. Direct Observation of the Local Reaction Environment during the Electrochemical Reduction of CO_2. *J. Am. Chem. Soc.* **2018**, *140* (22), 7012–7020.

(39) Nightingale, E. R. Phenomenological Theory of Ion Solvation. Effective Radii of Hydrated Ions. *J. Phys. Chem.* **1959**, *63* (9), 1381–1387.

Insert Table of Contents artwork here